Ultrafast Electron Transfer from CdSe Quantum Dots to a [FeFe]-Hydrogenase Mimic

Alexander Schleusener,[1,2] Mathias Micheel,[1] Stefan Benndorf,[3] Markus Rettenmayr,[4] Wolfgang Weigand,[3] Maria Wächtler[1,2]*

[1] Leibniz Institute of Photonic Technology, Department: Functional Interface, Albert-Einstein-Straße 9, 07745, Jena, Germany

[2] Institute of Physical Chemistry and Abbe Center of Photonics, Friedrich Schiller University Jena, Helmholtzweg 4, 07743, Jena, Germany

[3] Institute of Inorganic and Analytical Chemistry, Humboldtstraße 8, Friedrich Schiller University Jena, 07743 Jena, Germany

[4] Otto Schott Institute of Materials Research, Friedrich Schiller University Jena, Löbdergraben 32, 07743, Jena, Germany

Corresponding Author

*maria.waechtler@leibniz-ipht.de

ABSTRACT

The combination of CdSe nanoparticles as photosensitizers with [FeFe]-hydrogenase mimics is known to result in efficient systems for light-driven hydrogen generation with reported turnover numbers in the order of 10^4-10^6. Nevertheless, little is known about the details of the light-induced charge-transfer processes. Here we investigate the timescale of light-induced electron transfer kinetics for a simple model system consisting of CdSe quantum dots (QDs) of 2.0 nm diameter and a simple [FeFe]-hydrogenase mimic adsorbed to the QD surface under non-catalytic conditions. Our (time-resolved) spectroscopic investigation shows that both hot electron transfer on a sub-ps timescale and band-edge electron transfer on a sub-10-ps timescale from photoexcited QDs to adsorbed [FeFe]-hydrogenase mimics occurs. Fast recombination via back-electron-transfer is observed in the absence of a sacrificial agent or protons, which, under real catalytic conditions, would quench remaining holes or could stabilize the charge separation, respectively.

TOC GRAPHICS

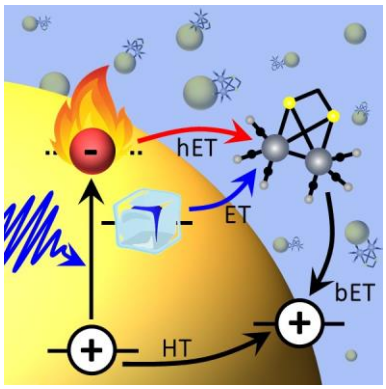

KEYWORDS colloidal semiconductor nanostructure, transient absorption spectroscopy, hot electron transfer, light-driven hydrogen generation, photocatalysis

Nanoparticles based on cadmium chalcogenides, in particular CdSe, have attracted considerable attention in the past decades as photoactive materials in photocatalysis.[1–3] They exhibit high absorption coefficients in the visible region and a rich surface chemistry, all of which can be tuned by changing synthesis parameters and, accordingly, size and shape of the particles. Absorption of a photon generates an exciton, which can dissociate into free charge carriers and the charges can directly be transferred to a substrate,[4] i.e., the nanoparticle itself acts as catalyst, or to a cocatalyst supporting the catalytic reaction, i.e. the nanoparticle acts as photosensitizer.[5–7] Catalytic centers, which have been coupled to CdSe nanoparticles, include metal nanoparticles, semiconductor nanoparticles, or molecular catalysts.[8] For use in artificial photosynthesis and as reduction center in the hydrogen evolution reaction, [FeFe]- and [NiFe]-hydrogenase enzymes (H_2ases) have been thoroughly investigated with cadmium chalcogenide nanoparticles as sensitizer.[9–12] These systems have been widely probed for their photon-to-hydrogen conversion efficiencies and displayed high turnover numbers (TONs) of 10^6 with CdSe@CdS nanorods as photosensitizer and a molecular redox-mediator.[13].

Despite the huge potential in this sensitizer-cocatalyst combination, the principal mechanistic steps underlying the light-driven catalytic mechanism are still under investigation. In particular, time-resolved spectroscopic studies elucidating the relevant charge transfer processes have only gained traction in the past few years. These mostly focused on nanosecond or longer timescales.[14–22] Charge transfer to H_2ase enzymes was found to occur on the nanosecond timescale with rate constants of electron transfer in the range of 10^6-10^9 s^{-1}.[16–19,23] Here, the slow interfacial electron transfer from the nanoparticle surface to the enzyme is limiting the efficiency of hydrogen generation due to the competition with exciton recombination on the same timescale. Small molecular redox-mediators, which shuttle charges from the excited semiconductor particle to the

enzyme, have been successfully used to enhance hydrogen conversion efficiency.[10,13,19,24] Critical parameters to consider are the distance to the catalytic center, which is influenced by the nature of the surface-capping ligands,[19] the structure of the enzyme itself,[25] and the number of adsorbed enzymes per nanocrystal. This becomes particularly important for quantum dots (QDs), which are comparable in size to H_2ases and have only limited surface area for enzyme adsorption.[25] Thus, combining QDs and so-called H_2ase mimics, which are simple and small molecular structures derived from the catalytic center of H_2ase,[11] has become a promising approach and TONs of 10^4-10^5 for CdSe QDs as photosensitizer have been reported.[14,15,22]

Reported rates of electron transfer to H_2ase mimics are also in the range of nanoseconds but remain only estimates based on Stern-Volmer analyses of photoluminescence (PL) quenching and time-resolved PL or transient absorption (TA) spectroscopy with nanosecond resolution. In the Stern-Volmer analysis, the quenching process is usually treated as a dynamic (diffusion controlled) process, yielding bimolecular quenching constants at low H_2ase mimic concentrations,[14,26] while static quenching due to adsorption of the mimic to the surface is often not considered. For a CdSe QD-H_2ase mimic assembly, a rate constant of ~10^7 s^{-1} was estimated based on ns-TA spectroscopy,[22] but this value only offers a lower limit of the actual electron transfer rate, as the recorded decay trace of the QD:H_2ase mimic complex lay within the response function of the detector. In particular, it is known that electron transfer from photoexcited cadmium chalcogenide nanoparticles to surface-proximal small organic molecules can occur on a tens of picoseconds or faster timescale.[27–34] However, this timescale has never been probed for a system of small [FeFe]-H_2ase mimics and CdSe QDs.

This lack of insight into the actual electron transfer step from the QD to the H_2ase mimic motivated us to conduct a fundamental study of the light-induced electron transfer step in a model

system consisting of CdSe QDs and the simple H_2ase mimic 1,3-(μ-propanedithiolato)diironhexacarbonyl (HM) (Figure 1A) employing steady-state and ns-time-resolved PL as well as fs-TA spectroscopy. To focus solely on the electron transfer step in the absence of catalytic activity, the investigation was performed in inert solvent (toluene) and in absence of any sacrificial agent. HM does not possess any defined binding groups, e.g. thiols, which excludes changes in the observed exciton dynamics caused by trap state upon binding of the anchoring group to the QD surface.[35–38] However, even in the absence of covalent binding, our investigations show that a stable complex (on the timescale of the investigated processes) between HM and the QD is formed, giving rise to a static quenching process and electron transfer on a sub-100-ps timescale.

CdSe QDs were synthesized by the hot-injection method.[39] Their absorption spectrum in toluene (Figure **1**A) shows three characteristic transitions at 360, 418, and 463 nm. These are ascribed to the $1P_e$-$1P_{3/2}$(h) (subsequently referred to as 1P), $1S_e$-$2S_{3/2}$(h) (2S) and $1S_e$-$1S_{3/2}$(h) (1S) transitions, respectively.[40] From the absorption peak position of the 1S transition, size and absorption coefficient ε of the QDs were derived,[41] yielding a particle diameter of 2.0 nm and $\varepsilon_{463} = 3.9 \times 10^4$ M^{-1} cm^{-1}. A complementary transmission electron microscopic analysis yields a diameter of (1.9 ± 0.7) nm (SI Figure S1 and S2). The absorption spectrum of HM (Figure **1**A) exhibits a sharp and strong (ε_{330} = 13500 M^{-1} cm^{-1}) absorption in the UV (λ_{max} = 330 nm) and broad, considerably weaker (ε_{465} = 1200 M^{-1} cm^{-1}) absorption in the UV/Vis (λ_{max} = 465 nm). These features are assigned to metal-to-ligand- and metal-to-metal-charge-transfer transitions, respectively.[42–44]

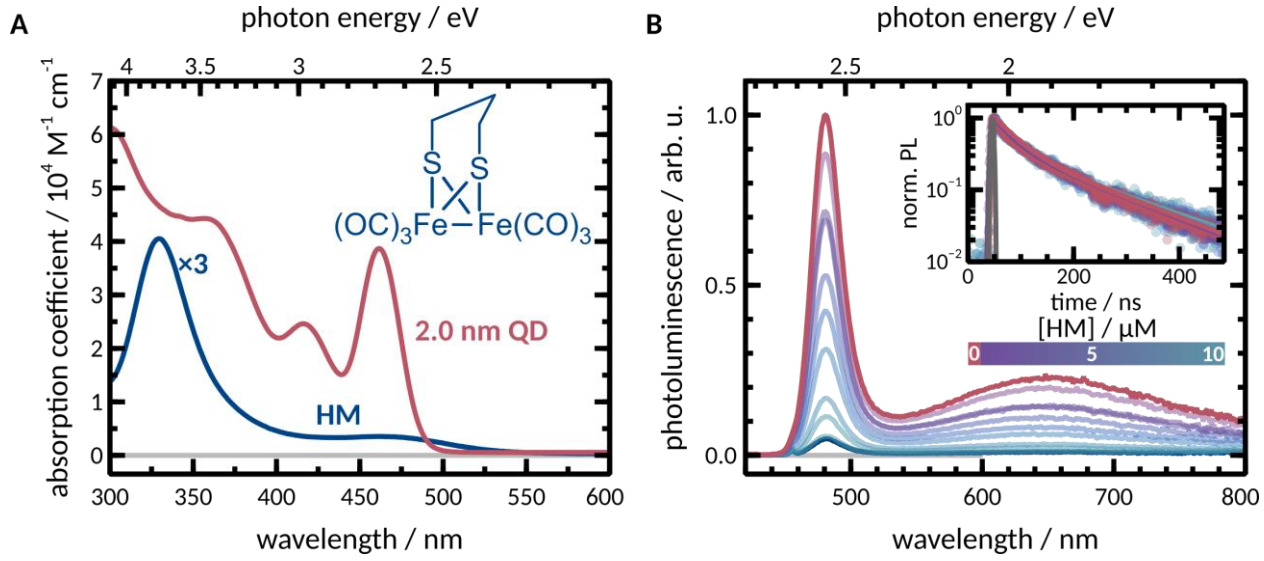

Figure 1. Absorption and photoluminescence (PL) spectroscopy of QDs in presence and absence of HM. A. Absorption spectra of 2.0 nm CdSe QD (red) and HM (blue, structure shown) recorded in toluene. The spectrum of HM was scaled by a factor of 3 for better visibility. B. Steady-state PL (λ_{ex} = 400 nm) of QDs at various HM concentrations. The inset shows time-resolved PL (λ_{ex} = 390 nm) of QDs recorded at different HM concentrations. Data points are shown as semi-transparent points, while a biexponential fit is shown as a solid curve. The grey line indicates the instrumental response function (FWHM = 1 ns). For all PL experiments, c_{QD} = c = 1.83 µM.

The QD PL spectrum (λ_{ex} = 400 nm) is characterized by a narrow PL band, which is only slightly red-shifted (λ_{max} = 480 nm) from the lowest energy absorption maximum, and a very broad, more pronouncedly red-shifted (λ_{max} = 655 nm) band extending to the near-infrared (**1**B). The narrow band corresponds to band-edge PL from the recombination of conduction band electrons with holes located in the valence band, while the broad band originates from trap- or surface-state PL due to radiative recombination of electrons and holes trapped in vacancies, usually attributed to undersaturated surface ions.[45]

In presence of HM, which is not photoluminescent itself, the spectral shape of PL remains unchanged (Figure **1**B). However, both band-edge and surface-state PL is quenched upon addition of HM. A Stern-Volmer plot of the integrated PL at different HM concentrations reveals a complex quenching behavior with a linear relationship only at HM concentrations below 5 µM, i.e., a ratio QD:HM of 1:3 (SI Figure S3). To gain further understanding of the quenching process, time-resolved PL was recorded (Figure **1**B, inset). PL of pure QDs exhibits a bimodal decay with time constants and corresponding amplitudes $\tau_{PL,1}$ = 40 ns (A_1 = 0.65) and $\tau_{PL,2}$ = 157 ns (A_2 = 0.35). The fast decay represents the radiative recombination of band-edge electrons and holes, while the slower decay is a result of thermal equilibration between the populations of so-called shallow trap states and of the band-edge.[46–48] The PL decay recorded at different HM concentrations (in the range from 0 to 10 µM) does not differ significantly from that recorded in the absence of HM (Figure **1**B, inset) with time constants and corresponding (relative) amplitudes remaining virtually unchanged (see SI Figure S4 and Table S1**Fehler! Verweisquelle konnte nicht gefunden werden.**). A quencher-concentration independent PL decay suggests a static quenching mechanism, where only surface-adsorbed HM quenches PL on a timescale well below the time-resolution of the setup of 1 ns.[49] Even though HM does not contain any specific moiety for surface binding such as thiols or amines, previous reports already demonstrated that for colloidal semiconductor nanocrystals, static quenching to an adsorbed, not covalently bound quencher occurs on a ps-timescale.[27–32,34] Diffusion-controlled quenching, on the other hand, occurs on a µs timescale, much longer than the exciton lifetime in the CdSe QDs investigated.

These sub-ns photoexcited dynamics of the CdSe QDs were subsequently investigated by TA spectroscopy with a sub-100-fs time-resolution in the absence and presence of HM. The ratio of QD:HM of 1:1 was chosen in the linear regime of the SV analysis of the steady-state PL (SI Figure

S3). Samples were excited at 390 nm with sufficiently low power densities to prevent excessive generation of multiple excitons per QD, which would show as an additional decay component due to, e.g., Auger recombination,[50] and probed with a white-light continuum ranging from 350 to 750 nm up to delay times of 1800 ps. Both pure QD and QD:HM were measured in inert atmosphere under identical conditions, i.e., same QD concentration and laser fluence, to ensure comparability of the data.

TA spectra of pure QDs (Figure 2A) are mainly characterized by two negative features peaking at 400 and 450 nm, respectively. By comparison with steady-state absorption, these are assigned to bleaching due to state filling of the 2S and 1S transitions.[51,52] Additionally, an intense photo-induced absorption (PIA) and a comparatively weak PIA were recorded at 480 nm and in the wavelength range 520-750 nm, respectively. The positive feature at 480 nm is ascribed to the "biexciton effect": when the excitation fluence is adjusted to mainly generate single excitons in the QDs, absorption of the probe pulse to the $1S_e$ level leads to the generation of a second exciton. The (attractive) interaction between these pump-pulse- and probe-pulse-generated excitons lowers the 1S transition energy and, accordingly, leads to a PIA which is bathochromically shifted from the ground-state absorption maximum.[53,54] The broad, minute PIA between 520 and 750 nm has been attributed to surface-localized ("trapped") holes.[55,56] Both bleach features increase in amplitude within the first 100s of fs after excitation, while the signal associated with trapped holes increases. After these initial dynamics, all signals partially decay until the end of our detection window (1800 ps).

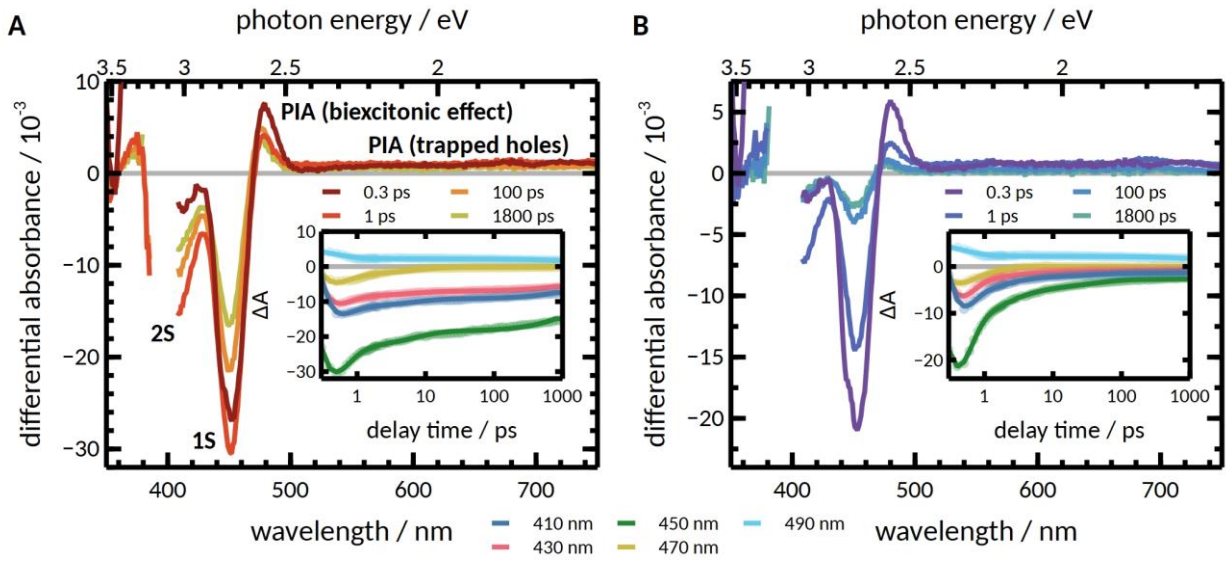

Figure 2. TA spectroscopy of 2.0 nm CdSe QDs in (A) absence and (B) presence of equimolar amounts of HM. Transient spectra were recorded at the specified delay times. The inset depicts kinetic traces (points represent data and straight lines represent the modeling on the basis of a multiexponential fit) at selected wavelengths. For QD:HM, the "parallel" model was used (see text).

The temporal and spectral evolution of the TA data was analyzed via global analysis. As for non-passivated QDs, the temporal evolution of the bleach region represents the electron population in the conduction band[57–59] and the weak photo-induced absorption represents the population of trapped holes, the spectral regions of 400-500 (2S and 1S bleach and PIA from the biexciton effect) and 550-680 nm (trapped holes) were fitted separately to account for the different origins of the observed dynamics.

The bleach recovery dynamics in pure QDs are best represented by four exponential terms (with the fourth time constant indicating a decay longer than our observation window of 1800 ps). It has to be noted that the assignment of time constants and corresponding amplitudes to specific processes is not straightforward in CdSe nanocrystals,[46,59] but it still presents a quantitative basis

for the subsequent discussion. The first process, an instrument-limited ($\tau_1 < 200$ fs) increase of the bleach amplitude, corresponds to the intraband "cooling" of "hot" electrons: as 390 nm excitation does not selectively address a single electronic transition, multiple transitions to higher electronic states are addressed in the QD ensemble. These quickly "cool down" to the band-edge of the $1P_e$, $2S_e$, and $1S_e$ levels, respectively.[60] The bleach then decays with $\tau_2 = (0.4 \pm 0.1)$ ps and $\tau_3 = (9.6 \pm 3.9)$ ps, which correspond to electrons being trapped to shallow and deep trap states.[56,61–64] Recombination of biexcitons, which were produced in small concentrations under the low laser fluence as well, occurs on a similar timescale: the kinetics recorded at ca. 470 nm, i.e., the zero-crossing between S1 bleach and PIA of the TA spectrum at long delay times, is indicative of biexciton recombination[54] and yields a biexciton recombination rate in the order of $(2 \text{ ps})^{-1}$. Finally, $\tau_4 > 1800$ ps describes the radiative and non-radiative recombination of excitons on a timescale longer than our observation window.

TA spectra recorded for the QD:HM system are qualitatively not different from those in the absence of HM, i.e., are characterized by negative contributions of the 2S and 1S bleaches, and PIA from the biexciton effect and trapped holes. However, all signal contributions are less intense and, additionally, decay considerably faster than recorded for pure QD. Comparison of transient spectra recorded in absence and presence of HM at a delay time of 600 fs, i.e., the minimum of the bleach build-up, shows that the amplitudes for the 1S and 2S bleaches in QD:HM are 30 % less than those of pure QD (Figure 3A). The QD concentration in both experiments was identical and the contribution of absorption of HM at the excitation wavelength, which could reduce response, is negligible. Similar effects have been observed in, e.g., metal nanoparticle tipped or molecularly functionalized systems, and have been related to ultra-fast transfer within the instrument resolution, e.g. originating from hot electron transfer.[65–67] The photon energy of the excitation

pulse is sufficient to initially excite higher excitonic levels. A fast transfer of conduction band electrons competing with intraband relaxation to the band edge reduces the population of the band edge states and, hence, reduces the bleach signal intensity after the initial cooling process.

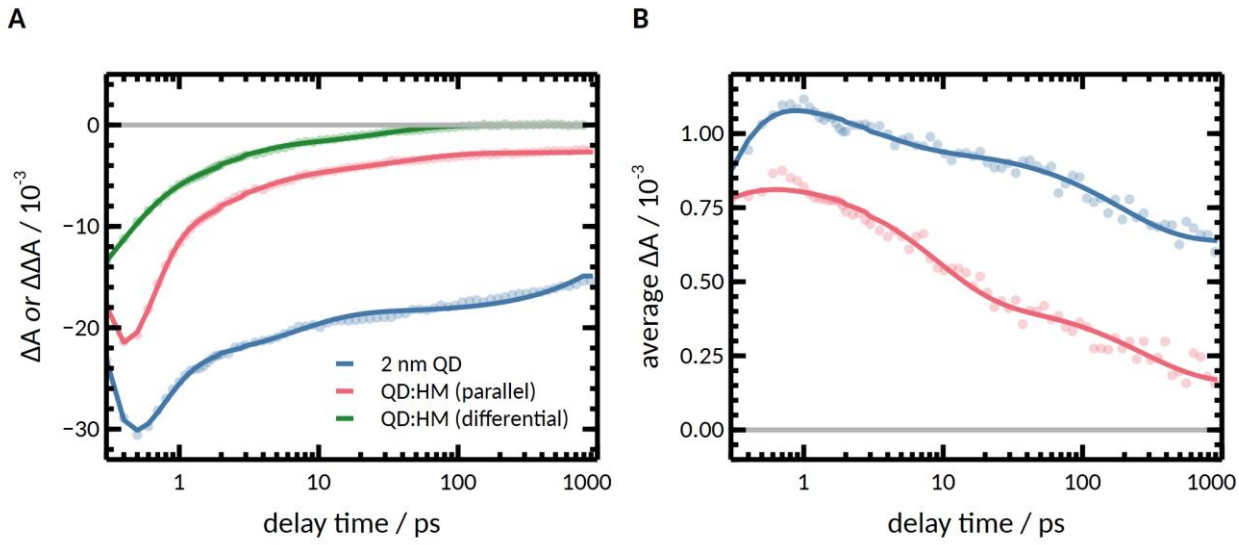

Figure 3. Kinetic traces of (A) bleach recovery (recorded at 450 nm) and (B) trapped holes (averaged from 550 to 680 nm). Data points are shown as points, whereas multiexponential fits are shown as solid lines.

Second, bleach recovery is significantly faster for QD:HM than for pure QD. However, comparison of normalized kinetic traces recorded at delay times >100 ps reveals that the excited state decay at longer delay times is not affected by the presence of HM (see SI Figure S5). This is in accordance with the unchanged recombination kinetics probed by time-resolved PL on the nanosecond timescale: only QDs with proximal HM undergo accelerated excited state decay, while the excited state decay of the remaining QDs is unchanged. In the TA spectroscopy experiment, both populations, i.e. QDs with and without HM, are excited. Thus, in order to unravel the electron transfer kinetics to HM, the population of unquenched photoexcited QD has to be taken into consideration. Here, we used two complementary models: in the first (subsequently referred to as

"parallel"), we assume two additional, parallel decays from the initially "cool" excited state, while the decay of pure QDs is scaled by a factor x representing residual QDs which are not quenched. In the second model ("differential"), we subtract the fitted data derived for pure QDs from the QD:HM measurement scaled by $\Delta A(1000\ ps)_{QD:HM}/\Delta A(1000\ ps)_{QD}$ (Figure S9). In both models, a three-exponential decay was needed to satisfactorily represent the data. It is important to note that a multiexponential decay cannot be distinguished from a lifetime distribution which has also been presented in previous reports on the interaction of photoexcited QDs by molecular quenchers.[68] For the parallel approach, one obtains $\tau_{1,p}' < 0.2$ ps, $\tau_{2,p}' = (0.3 \pm 0.1)$ ps and $\tau_{3,p}' = (3.8 \pm 1.8)$ ps, and for the differential one $\tau_{1,d}' = (0.3 \pm 0.1)$ ps, $\tau_{2,d}' = (2.7 \pm 1.6)$ ps and $\tau_{3,d}' = (36.8 \pm 8.6)$ ps (SI Table S2). We interpret the sub-ps time constants ($\tau_{1,p}'$, $\tau_{2,p}'$ and $\tau_{1,d}'$) as the timescale of hot electron transfer to HM, which efficiently competes with intraband cooling. The distinctively slower electron transfer (represented by $\tau_{3,p}'$, $\tau_{2,d}'$ and $\tau_{3,d}'$) on a picosecond timescale then describes the transfer from the relaxed band edge states.[27,69] Also contributions from shallow surface trap sites cannot be ruled out in this investigation: for CdTe/CdS core-shell QD with an electron acceptor covalently bound to the surface, electron transfer rates from surface trap states in the order of $(2\text{-}8\ ps)^{-1}$ have been identified,[67] a view substantiated by theoretical modeling.[70] Thus, electron transfer might occur both from the band-edge as well as from shallow trap states.

So far, we have only considered the transient signals reporting on population of conduction band levels with electrons. The PIA signal spanning 550-680 nm reports on the dynamics of holes trapped in surface states (Figure 2B). This signal is formed with a rise time of < 0.2 ps. In absence of the HM, this signal decay can be described by two time constants of (103 ± 8) and >1800 ps. The decay is attributed to recombination with conduction band electrons.[46] Similar to the 2S and 1S bleach signals, the amplitude of the PIA signal is reduced in presence of HM. Due to the

energetic band position, a direct ultrafast hole transfer to HM is ruled out and the reduction of the trapped-hole PIA amplitude might be due to (weak) surface passivation of adsorbed HM. An acceleration of the PIA signal decay in the QD:HM complex compared to the pure QDs is observed. Here, the decay was modelled only using the parallel approach, as the decay of the trapped hole PIA at long delay times in presence and absence of HM differ significantly (Figure S10). A single time constant of (10.1 ± 0.4) ps was obtained. We interpret this acceleration as indication of recombination processes between the electrons transferred to HM and holes trapped in surface defect sites. It has already been shown for CdSe QDs that an ultrafast (2 ps) electron transfer to an adsorbed organic acceptor is followed by a slower back-electron-transfer to shallow hole traps on a timescale of tens of ps.[32] As our experiments were conducted in the absence of any additional hole scavenger, this back-electron transfer is also feasible here.

In summary, these results show that, if contact is sufficiently close between a QD and a [FeFe]-H_2ase mimic, electron transfer from photoexcited QDs to [FeFe]-H_2ase mimics can occur on a sub-10-ps timescale and even transfer of hot electrons on the sub-200-fs timescale is possible. Further, we observed fast recombination of the electron transferred to HM and holes trapped at surface defects of the QD. (Scheme 1). Our experiments were performed in inert solvent an in absence of sacrificial agents that are typically available under catalytic conditions. The interaction with protons in the real reaction medium and fast quenching of trapped holes can contribute to a stabilization of the charge at transferred to the [FeFe]-H_2ase mimic. Future studies should increase the complexity of the environment and address these additional interactions and their impact on the charge transfer efficiency and rate and the lifetime of charge separation under conditions closer to an actual catalytic experiment.

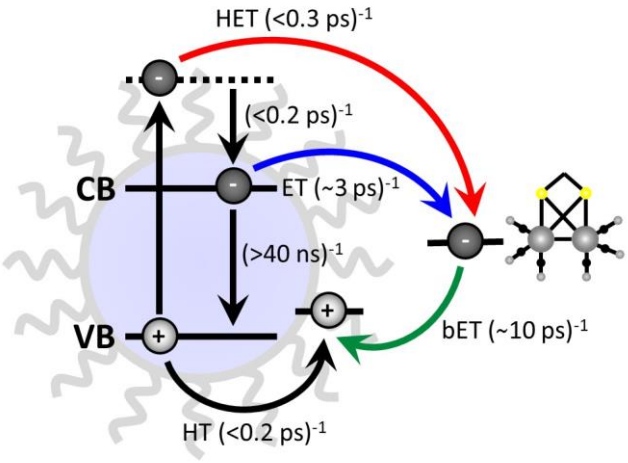

Scheme 1. Summary of the interaction of a CdSe QD with HM. In the absence of HM, an electron is promoted to the conduction band (CB), while a hole is left in the valence band (VB). The "hot" electron quickly relaxes to the band edge and the hole is trapped (HT) on a similar timescale. The excited QD returns back to the ground state on a nanosecond timescale. With a proximal HM, hot electron transfer (HET) efficiently competes with intraband cooling. Another electron transfer (ET) step to HM also efficiently competes with band-edge recombination, while back-electron transfer (bET) to trapped surface holes also occurs on a timescale of ~10 ps.

ASSOCIATED CONTENT

Supporting Information. The following files are available free of charge. Details on the synthesis of HM and QDs, experimental procedures, TEM analysis, PL Quenching, PL lifetime measurements and the fitting procedure of the TA data is supplied in the supplementary material (pdf).

AUTHOR INFORMATION

Notes

The authors declare no competing financial interests.

ACKNOWLEDGMENT

This research was funded by the German Research Foundation (DFG)—project number 364549901—TRR234 (CataLight, A2, B4 and Z2), Inst 275/391-1, and the Fonds der Chemischen Industrie (FCI). We thank Dipl.-Ing. Hans-Jürgen Hempel for performing the TEM measurements.

REFERENCES

(1) Weiss, E. A. Designing the Surfaces of Semiconductor Quantum Dots for Colloidal Photocatalysis. *ACS Energy Lett.* **2017**, *2* (5), 1005–1013. https://doi.org/10.1021/acsenergylett.7b00061.

(2) Burke, R.; Bren, K. L.; Krauss, T. D. Semiconductor Nanocrystal Photocatalysis for the Production of Solar Fuels. *J. Chem. Phys.* **2021**, *154* (3), 030901. https://doi.org/10.1063/5.0032172.

(3) Li, X.-B.; Tung, C.-H.; Wu, L.-Z. Semiconducting Quantum Dots for Artificial Photosynthesis. *Nature Reviews Chemistry* **2018**, *2* (8), 160–173. https://doi.org/10.1038/s41570-018-0024-8.

(4) Lu, H.; Huang, Z.; Martinez, M. S.; Johnson, J. C.; Luther, J. M.; Beard, M. C. Transforming Energy Using Quantum Dots. *Energy Environ. Sci.* **2020**, *13* (5), 1347–1376. https://doi.org/10.1039/C9EE03930A.

(5) Wang, M.; Han, K.; Zhang, S.; Sun, L. Integration of Organometallic Complexes with Semiconductors and Other Nanomaterials for Photocatalytic H2 Production. *Coordination Chemistry Reviews* **2015**, *287*, 1–14. https://doi.org/10.1016/j.ccr.2014.12.005.

(6) Wang, Q.; Domen, K. Particulate Photocatalysts for Light-Driven Water Splitting: Mechanisms, Challenges, and Design Strategies. *Chem. Rev.* **2020**, *120* (2), 919–985. https://doi.org/10.1021/acs.chemrev.9b00201.

(7) Xu, Y.; Huang, Y.; Zhang, B. Rational Design of Semiconductor-Based Photocatalysts for Advanced Photocatalytic Hydrogen Production: The Case of Cadmium Chalcogenides. *Inorg. Chem. Front.* **2016**, *3* (5), 591–615. https://doi.org/10.1039/C5QI00217F.

(8) Zhang, B.; Sun, L. Artificial Photosynthesis: Opportunities and Challenges of Molecular Catalysts. *Chemical Society Reviews* **2019**, *48* (7), 2216–2264. https://doi.org/10.1039/C8CS00897C.

(9) Wild, A.; Teichler, A.; Ho, C. L.; Wang, X. Z.; Zhan, H. M.; Schlutter, F.; Winter, A.; Hager, M. D.; Wong, W. Y.; Schubert, U. S. Formation of Dynamic Metallo-Copolymers

by Inkjet Printing: Towards White-Emitting Materials. *J. Mater. Chem. C* **2013**, *1* (9), 1812–1822. https://doi.org/10.1039/c2tc00552b.

(10) Brown, K. A.; Wilker, M. B.; Boehm, M.; Dukovic, G.; King, P. W. Characterization of Photochemical Processes for H2 Production by CdS Nanorod–[FeFe] Hydrogenase Complexes. *J. Am. Chem. Soc.* **2012**, *134* (12), 5627–5636. https://doi.org/10.1021/ja2116348.

(11) Watanabe, M.; Honda, Y.; Hagiwara, H.; Ishihara, T. [FeFe]-Hydrogenase and Its Organic Molecule Mimics—Artificial and Bioengineering Application for Hydrogenproduction. *Journal of Photochemistry and Photobiology C: Photochemistry Reviews* **2017**, *33*, 1–26. https://doi.org/10.1016/j.jphotochemrev.2017.09.001.

(12) Troppmann, S.; König, B. Functionalized Vesicles with Co-Embedded CdSe Quantum Dots and [FeFe]-Hydrogenase Mimic for Light-Driven Hydrogen Production. *ChemistrySelect* **2016**, *1* (7), 1405–1409. https://doi.org/10.1002/slct.201600032.

(13) Chica, B.; Wu, C.-H.; Liu, Y.; Adams, M. W. W.; Lian, T.; Dyer, R. B. Balancing Electron Transfer Rate and Driving Force for Efficient Photocatalytic Hydrogen Production in CdSe/CdS Nanorod–[NiFe] Hydrogenase Assemblies. *Energy Environ. Sci.* **2017**, *10* (10), 2245–2255. https://doi.org/10.1039/C7EE01738C.

(14) Jian, J.-X.; Ye, C.; Wang, X.-Z.; Wen, M.; Li, Z.-J.; Li, X.-B.; Chen, B.; Tung, C.-H.; Wu, L.-Z. Comparison of H2 Photogeneration by [FeFe]-Hydrogenase Mimics with CdSe QDs and Ru(Bpy)3Cl2 in Aqueous Solution. *Energy Environ. Sci.* **2016**, *9* (6), 2083–2089. https://doi.org/10.1039/C6EE00629A.

(15) Wen, M.; Li, X.-B.; Jian, J.-X.; Wang, X.-Z.; Wu, H.-L.; Chen, B.; Tung, C.-H.; Wu, L.-Z. Secondary Coordination Sphere Accelerates Hole Transfer for Enhanced Hydrogen Photogeneration from [FeFe]-Hydrogenase Mimic and CdSe QDs in Water. *Sci Rep* **2016**, *6* (1), 1–8. https://doi.org/10.1038/srep29851.

(16) Wilker, M. B.; Shinopoulos, K. E.; Brown, K. A.; Mulder, D. W.; King, P. W.; Dukovic, G. Electron Transfer Kinetics in CdS Nanorod–[FeFe]-Hydrogenase Complexes and Implications for Photochemical H2 Generation. *J. Am. Chem. Soc.* **2014**, *136* (11), 4316–4324. https://doi.org/10.1021/ja413001p.

(17) Utterback, J. K.; Wilker, M. B.; Mulder, D. W.; King, P. W.; Eaves, J. D.; Dukovic, G. Quantum Efficiency of Charge Transfer Competing against Nonexponential Processes: The Case of Electron Transfer from CdS Nanorods to Hydrogenase. *J. Phys. Chem. C* **2019**, *123* (1), 886–896. https://doi.org/10.1021/acs.jpcc.8b09916.

(18) Utterback, J. K.; Wilker, M. B.; Brown, K. A.; King, P. W.; Eaves, J. D.; Dukovic, G. Competition between Electron Transfer, Trapping, and Recombination in CdS Nanorod–Hydrogenase Complexes. *Phys. Chem. Chem. Phys.* **2015**, *17* (8), 5538–5542. https://doi.org/10.1039/C4CP05993J.

(19) Wilker, M. B.; Utterback, J. K.; Greene, S.; Brown, K. A.; Mulder, D. W.; King, P. W.; Dukovic, G. Role of Surface-Capping Ligands in Photoexcited Electron Transfer between CdS Nanorods and [FeFe] Hydrogenase and the Subsequent H2 Generation. *J. Phys. Chem. C* **2018**, *122* (1), 741–750. https://doi.org/10.1021/acs.jpcc.7b07229.

(20) Sanchez, M. L. K.; Sommer, C.; Reijerse, E.; Birrell, J. A.; Lubitz, W.; Dyer, R. B. Investigating the Kinetic Competency of CrHydA1 [FeFe] Hydrogenase Intermediate States via Time-Resolved Infrared Spectroscopy. *J. Am. Chem. Soc.* **2019**, *141* (40), 16064–16070. https://doi.org/10.1021/jacs.9b08348.

(21) Liang, W.-J.; Wang, F.; Wen, M.; Jian, J.-X.; Wang, X.-Z.; Chen, B.; Tung, C.-H.; Wu, L.-Z. Branched Polyethylenimine Improves Hydrogen Photoproduction from a CdSe Quantum Dot/[FeFe]-Hydrogenase Mimic System in Neutral Aqueous Solutions. *Chemistry – A European Journal* **2015**, *21* (8), 3187–3192. https://doi.org/10.1002/chem.201406361.
(22) Li, X.-B.; Jian, J.-X.; Wang, X.-Z.; Wang, Y.; Xia, S.-G.; Tung, C.-H.; Wu, L.-Z. Per-6-Thiol-Cyclodextrin Engineered [FeFe]-Hydrogenase Mimic/CdSe Quantum Dot Assembly for Photocatalytic Hydrogen Production. *Solar RRL* **2021**, *5* (2), 2000474. https://doi.org/10.1002/solr.202000474.
(23) Brown, K. A.; Song, Q.; Mulder, D. W.; King, P. W. Diameter Dependent Electron Transfer Kinetics in Semiconductor–Enzyme Complexes. *ACS Nano* **2014**, *8* (10), 10790–10798. https://doi.org/10.1021/nn504561v.
(24) Sanchez, M. L. K.; Wu, C.-H.; Adams, M. W. W.; Dyer, R. B. Optimizing Electron Transfer from CdSe QDs to Hydrogenase for Photocatalytic H2 Production. *Chem. Commun.* **2019**, *55* (39), 5579–5582. https://doi.org/10.1039/C9CC01150A.
(25) Utterback, J. K.; Ruzicka, J. L.; Keller, H. R.; Pellows, L. M.; Dukovic, G. Electron Transfer from Semiconductor Nanocrystals to Redox Enzymes. *Annu. Rev. Phys. Chem.* **2020**, *71* (1), 335–359. https://doi.org/10.1146/annurev-physchem-050317-014232.
(26) Cheng, M.; Wang, M.; Zhang, S.; Liu, F.; Yang, Y.; Wan, B.; Sun, L. Photocatalytic H2 Production Using a Hybrid Assembly of an [FeFe]-Hydrogenase Model and CdSe Quantum Dot Linked through a Thiolato-Functionalized Cyclodextrin. *Faraday Discuss.* **2017**, *198* (0), 197–209. https://doi.org/10.1039/C6FD00207B.
(27) Dworak, L.; Matylitsky, V. V.; Breus, V. V.; Braun, M.; Basché, T.; Wachtveitl, J. Ultrafast Charge Separation at the CdSe/CdS Core/Shell Quantum Dot/Methylviologen Interface: Implications for Nanocrystal Solar Cells. *J. Phys. Chem. C* **2011**, *115* (10), 3949–3955. https://doi.org/10.1021/jp111574w.
(28) Huang, J.; Mulfort, K. L.; Du, P.; Chen, L. X. Photodriven Charge Separation Dynamics in CdSe/ZnS Core/Shell Quantum Dot/Cobaloxime Hybrid for Efficient Hydrogen Production. *J. Am. Chem. Soc.* **2012**, *134* (40), 16472–16475. https://doi.org/10.1021/ja3062584.
(29) Knowles, K. E.; Malicki, M.; Weiss, E. A. Dual-Time Scale Photoinduced Electron Transfer from PbS Quantum Dots to a Molecular Acceptor. *J. Am. Chem. Soc.* **2012**, *134* (30), 12470–12473. https://doi.org/10.1021/ja3060222.
(30) Knowles, K. E.; Tagliazucchi, M.; Malicki, M.; Swenson, N. K.; Weiss, E. A. Electron Transfer as a Probe of the Permeability of Organic Monolayers on the Surfaces of Colloidal PbS Quantum Dots. *J. Phys. Chem. C* **2013**, *117* (30), 15849–15857. https://doi.org/10.1021/jp406485y.
(31) Liu, C.; Qiu, F.; Peterson, J. J.; Krauss, T. D. Aqueous Photogeneration of H2 with CdSe Nanocrystals and Nickel Catalysts: Electron Transfer Dynamics. *J. Phys. Chem. B* **2015**, *119* (24), 7349–7357. https://doi.org/10.1021/jp510935w.
(32) Thomas, A.; Sandeep, K.; Somasundaran, S. M.; Thomas, K. G. How Trap States Affect Charge Carrier Dynamics of CdSe and InP Quantum Dots: Visualization through Complexation with Viologen. *ACS Energy Lett.* **2018**, *3* (10), 2368–2375. https://doi.org/10.1021/acsenergylett.8b01532.
(33) Wang, Z.; Rafipoor, M.; Risueño, P. G.; Merkl, J.-P.; Han, P.; Lange, H.; Bester, G. Phonon-Assisted Auger Process Enables Ultrafast Charge Transfer in CdSe Quantum Dot/Organic

Molecule. *J. Phys. Chem. C* **2019**, *123* (28), 17127–17135. https://doi.org/10.1021/acs.jpcc.9b03348.
(34) Zeng, P.; Kirkwood, N.; Mulvaney, P.; Boldt, K.; A. Smith, T. Shell Effects on Hole-Coupled Electron Transfer Dynamics from CdSe/CdS Quantum Dots to Methyl Viologen. *Nanoscale* **2016**, *8* (19), 10380–10387. https://doi.org/10.1039/C6NR00168H.
(35) Micheel, M.; Liu, B.; Wächtler, M. Influence of Surface Ligands on Charge-Carrier Trapping and Relaxation in Water-Soluble CdSe@CdS Nanorods. *Catalysts* **2020**, *10* (10), 1143. https://doi.org/10.3390/catal10101143.
(36) Palato, S.; Seiler, H.; McGovern, L.; Mack, T. G.; Jethi, L.; Kambhampati, P. Electron Dynamics at the Surface of Semiconductor Nanocrystals. *J. Phys. Chem. C* **2017**, *121* (47), 26519–26527. https://doi.org/10.1021/acs.jpcc.7b09145.
(37) Peterson, M. D.; Cass, L. C.; Harris, R. D.; Edme, K.; Sung, K.; Weiss, E. A. The Role of Ligands in Determining the Exciton Relaxation Dynamics in Semiconductor Quantum Dots. *Annual Review of Physical Chemistry* **2014**, *65* (1), 317–339. https://doi.org/10.1146/annurev-physchem-040513-103649.
(38) Smith, A. M.; Duan, H.; Rhyner, M. N.; Ruan, G.; Nie, S. A Systematic Examination of Surface Coatings on the Optical and Chemical Properties of Semiconductor Quantum Dots. *Phys. Chem. Chem. Phys.* **2006**, *8* (33), 3895–3903. https://doi.org/10.1039/B606572B.
(39) Carbone, L.; Nobile, C.; De Giorgi, M.; Sala, F. D.; Morello, G.; Pompa, P.; Hytch, M.; Snoeck, E.; Fiore, A.; Franchini, I. R.; Nadasan, M.; Silvestre, A. F.; Chiodo, L.; Kudera, S.; Cingolani, R.; Krahne, R.; Manna, L. Synthesis and Micrometer-Scale Assembly of Colloidal CdSe/CdS Nanorods Prepared by a Seeded Growth Approach. *Nano Lett.* **2007**, *7* (10), 2942–2950. https://doi.org/10.1021/nl0717661.
(40) Caram, J. R.; Zheng, H.; Dahlberg, P. D.; Rolczynski, B. S.; Griffin, G. B.; Dolzhnikov, D. S.; Talapin, D. V.; Engel, G. S. Exploring Size and State Dynamics in CdSe Quantum Dots Using Two-Dimensional Electronic Spectroscopy. *J. Chem. Phys.* **2014**, *140* (8), 084701. https://doi.org/10.1063/1.4865832.
(41) Yu, W. W.; Qu, L.; Guo, W.; Peng, X. Experimental Determination of the Extinction Coefficient of CdTe, CdSe, and CdS Nanocrystals. *Chem. Mater.* **2003**, *15* (14), 2854–2860. https://doi.org/10.1021/cm034081k.
(42) Bingaman, J. L.; Kohnhorst, C. L.; Van Meter, G. A.; McElroy, B. A.; Rakowski, E. A.; Caplins, B. W.; Gutowski, T. A.; Stromberg, C. J.; Webster, C. E.; Heilweil, E. J. Time-Resolved Vibrational Spectroscopy of [FeFe]-Hydrogenase Model Compounds. *J. Phys. Chem. A* **2012**, *116* (27), 7261–7271. https://doi.org/10.1021/jp2121774.
(43) Kunkely, H.; Vogler, A. Photoreactivity of Fe2S2(CO)6 Originating from Dσ* Metal-to-Ligand Charge Transfer Excitation. *Journal of Organometallic Chemistry* **1998**, *568* (1), 291–293. https://doi.org/10.1016/S0022-328X(98)00846-8.
(44) Silaghi-Dumitrescu, I.; Bitterwolf, T. E.; King, R. B. Butterfly Diradical Intermediates in Photochemical Reactions of Fe2(CO)6(μ-S2). *J. Am. Chem. Soc.* **2006**, *128* (16), 5342–5343. https://doi.org/10.1021/ja061272q.
(45) Lim, S. J.; Ma, L.; Schleife, A.; Smith, A. M. Quantum Dot Surface Engineering: Toward Inert Fluorophores with Compact Size and Bright, Stable Emission. *Coordination Chemistry Reviews* **2016**, *320–321*, 216–237. https://doi.org/10.1016/j.ccr.2016.03.012.
(46) Knowles, K. E.; McArthur, E. A.; Weiss, E. A. A Multi-Timescale Map of Radiative and Nonradiative Decay Pathways for Excitons in CdSe Quantum Dots. *ACS Nano* **2011**, *5* (3), 2026–2035. https://doi.org/10.1021/nn2002689.

(47) Fitzmorris, B. C.; Cooper, J. K.; Edberg, J.; Gul, S.; Guo, J.; Zhang, J. Z. Synthesis and Structural, Optical, and Dynamic Properties of Core/Shell/Shell CdSe/ZnSe/ZnS Quantum Dots. *J. Phys. Chem. C* **2012**, *116* (47), 25065–25073. https://doi.org/10.1021/jp3092013.
(48) Kloepfer, J. A.; Bradforth, S. E.; Nadeau, J. L. Photophysical Properties of Biologically Compatible CdSe Quantum Dot Structures. *J. Phys. Chem. B* **2005**, *109* (20), 9996–10003. https://doi.org/10.1021/jp044581g.
(49) Valeur, B.; Berberan-Santos, M. N. *Molecular Fluorescence: Principles and Applications*, Second.; Wiley-VCH Verlag GmbH & Co. KGaA: Weinheim, Germany, 2012.
(50) Melnychuk, C.; Guyot-Sionnest, P. Multicarrier Dynamics in Quantum Dots. *Chem. Rev.* **2021**. https://doi.org/10.1021/acs.chemrev.0c00931.
(51) Wang, H.; de Mello Donegá, C.; Meijerink, A.; Glasbeek, M. Ultrafast Exciton Dynamics in CdSe Quantum Dots Studied from Bleaching Recovery and Fluorescence Transients. *J. Phys. Chem. B* **2006**, *110* (2), 733–737. https://doi.org/10.1021/jp055795g.
(52) Zhang, C.; Do, T. N.; Ong, X.; Chan, Y.; Tan, H.-S. Understanding the Features in the Ultrafast Transient Absorption Spectra of CdSe Quantum Dots. *Chemical Physics* **2016**, *481*, 157–164. https://doi.org/10.1016/j.chemphys.2016.08.027.
(53) Klimov, V. I. Spectral and Dynamical Properties of Multiexcitons in Semiconductor Nanocrystals. *Annu. Rev. Phys. Chem.* **2007**, *58* (1), 635–673. https://doi.org/10.1146/annurev.physchem.58.032806.104537.
(54) Labrador, T.; Dukovic, G. Simultaneous Determination of Spectral Signatures and Decay Kinetics of Excited State Species in Semiconductor Nanocrystals Probed by Transient Absorption Spectroscopy. *J. Phys. Chem. C* **2020**, *124* (15), 8439–8447. https://doi.org/10.1021/acs.jpcc.0c01701.
(55) Jasrasaria, D.; Philbin, J. P.; Yan, C.; Weinberg, D.; Alivisatos, A. P.; Rabani, E. Sub-Bandgap Photoinduced Transient Absorption Features in CdSe Nanostructures: The Role of Trapped Holes. *J. Phys. Chem. C* **2020**, *124* (31), 17372–17378. https://doi.org/10.1021/acs.jpcc.0c04746.
(56) Schnitzenbaumer, K. J.; Labrador, T.; Dukovic, G. Impact of Chalcogenide Ligands on Excited State Dynamics in CdSe Quantum Dots. *J. Phys. Chem. C* **2015**, *119* (23), 13314–13324. https://doi.org/10.1021/acs.jpcc.5b02880.
(57) Morgan, D. P.; Kelley, D. F. What Does the Transient Absorption Spectrum of CdSe Quantum Dots Measure? *J. Phys. Chem. C* **2020**, *124* (15), 8448–8455. https://doi.org/10.1021/acs.jpcc.0c02566.
(58) Grimaldi, G.; Geuchies, J. J.; van der Stam, W.; du Fossé, I.; Brynjarsson, B.; Kirkwood, N.; Kinge, S.; Siebbeles, L. D. A.; Houtepen, A. J. Spectroscopic Evidence for the Contribution of Holes to the Bleach of Cd-Chalcogenide Quantum Dots. *Nano Lett.* **2019**, *19* (5), 3002–3010. https://doi.org/10.1021/acs.nanolett.9b00164.
(59) Taheri, M. M.; Elbert, K. C.; Yang, S.; Diroll, B. T.; Park, J.; Murray, C. B.; Baxter, J. B. Distinguishing Electron and Hole Dynamics in Functionalized CdSe/CdS Core/Shell Quantum Dots Using Complementary Ultrafast Spectroscopies and Kinetic Modeling. *J. Phys. Chem. C* **2021**, *125* (1), 31–41. https://doi.org/10.1021/acs.jpcc.0c07037.
(60) Hendry, E.; Koeberg, M.; Wang, F.; Zhang, H.; de Mello Donegá, C.; Vanmaekelbergh, D.; Bonn, M. Direct Observation of Electron-to-Hole Energy Transfer in CdSe Quantum Dots. *Phys. Rev. Lett.* **2006**, *96* (5), 057408. https://doi.org/10.1103/PhysRevLett.96.057408.

(61) Klimov, V. I.; McBranch, D. W.; Leatherdale, C. A.; Bawendi, M. G. Electron and Hole Relaxation Pathways in Semiconductor Quantum Dots. *Phys. Rev. B* **1999**, *60* (19), 13740–13749. https://doi.org/10.1103/PhysRevB.60.13740.

(62) Boehme, S. C.; Walvis, T. A.; Infante, I.; Grozema, F. C.; Vanmaekelbergh, D.; Siebbeles, L. D. A.; Houtepen, A. J. Electrochemical Control over Photoinduced Electron Transfer and Trapping in CdSe-CdTe Quantum-Dot Solids. *ACS Nano* **2014**, *8* (7), 7067–7077. https://doi.org/10.1021/nn501985e.

(63) Saari, J. I.; Dias, E. A.; Reifsnyder, D.; Krause, M. M.; Walsh, B. R.; Murray, C. B.; Kambhampati, P. Ultrafast Electron Trapping at the Surface of Semiconductor Nanocrystals: Excitonic and Biexcitonic Processes. *J. Phys. Chem. B* **2013**, *117* (16), 4412–4421. https://doi.org/10.1021/jp307668g.

(64) McArthur, E. A.; Morris-Cohen, A. J.; Knowles, K. E.; Weiss, E. A. Charge Carrier Resolved Relaxation of the First Excitonic State in CdSe Quantum Dots Probed with Near-Infrared Transient Absorption Spectroscopy. *J. Phys. Chem. B* **2010**, *114* (45), 14514–14520. https://doi.org/10.1021/jp102101f.

(65) Mondal, N.; Samanta, A. Ultrafast Charge Transfer and Trapping Dynamics in a Colloidal Mixture of Similarly Charged CdTe Quantum Dots and Silver Nanoparticles. *J. Phys. Chem. C* **2016**, *120* (1), 650–658. https://doi.org/10.1021/acs.jpcc.5b08630.

(66) Okuhata, T.; Katayama, T.; Tamai, N. Ultrafast and Hot Electron Transfer in CdSe QD–Au Hybrid Nanostructures. *J. Phys. Chem. C* **2020**, *124* (1), 1099–1107. https://doi.org/10.1021/acs.jpcc.9b09042.

(67) Harvie, A. J.; Smith, C. T.; Ahumada-Lazo, R.; Jeuken, L. J. C.; Califano, M.; Bon, R. S.; Hardman, S. J. O.; Binks, D. J.; Critchley, K. Ultrafast Trap State-Mediated Electron Transfer for Quantum Dot Redox Sensing. *J. Phys. Chem. C* **2018**, *122* (18), 10173–10180. https://doi.org/10.1021/acs.jpcc.8b02551.

(68) Morris-Cohen, A. J.; Frederick, M. T.; Cass, L. C.; Weiss, E. A. Simultaneous Determination of the Adsorption Constant and the Photoinduced Electron Transfer Rate for a Cds Quantum Dot–Viologen Complex. *J. Am. Chem. Soc.* **2011**, *133* (26), 10146–10154. https://doi.org/10.1021/ja2010237.

(69) Huang, J.; Stockwell, D.; Huang, Z.; Mohler, D. L.; Lian, T. Photoinduced Ultrafast Electron Transfer from CdSe Quantum Dots to Re-Bipyridyl Complexes. *J. Am. Chem. Soc.* **2008**, *130* (17), 5632–5633. https://doi.org/10.1021/ja8003683.

(70) Califano, M. Charge Dynamics in Quantum-Dot–Acceptor Complexes in the Presence of Confining and Deconfining Ligands. *J. Phys. Chem. Lett.* **2020**, *11* (1), 280–285. https://doi.org/10.1021/acs.jpclett.9b03073.

Supporting Information

Experimental

Synthesis

Synthesis [FeFe] H_2ase mimic HM – 1,3-(μ-propanedithiolato)diironhexacarbonyl was synthesized by a modified procedure from Huttner and coauthors.[1] A stirred solution of 0.466 g triiron dodecacarbonyl and 0.1 g 1,3-propanedithiol in 20 ml dry toluene was heated to 80 °C for 1 hour under nitrogen atmosphere. The resulting brown mixture was concentrated under reduced pressure and purified by column chromatography (eluent: cyclohexane) to get 0.285 g (yield 80 %) of a red solid from the mayor red band.

^{1}H-NMR (600 MHz, CD_2Cl_2, 297 K) δ (ppm) = 2.16 (br s, 2H), 1.80 (br s, 1H).

^{13}C {^{1}H}-NMR (151 MHz, CD_2Cl_2, 297 K) δ (ppm) = 208.6, 30.9, 23.8.

Synthesis Quantum dots – CdSe quantumdots were synthesized adopting a protocol published by Manna and coauthors.[2] 3.0g of Trioctylphosphine oxide (TOPO), 0.280g of Octadecylphosphonic acid (ODPA) and 60mg of Cadmium Oxide (CdO) are mixed in a 25ml three-neck flask, heated to 150°C and exposed to vacuum for 1 hour. Then, under nitrogen, the solution is heated to 300°C to dissolve the CdO until it turns optically clear and colorless. At this point, 1.5g of Trioctylphosphine (TOP) is injected into the flask. The temperature is raised to 350°C, and TOP:Se solution (0.058g Se + 0.360g TOP) is injected and the reaction mixture immediately cooled down by removing the heating mantle. After the synthesis, the nanocrystals are precipitated with methanol, and are washed three times in total by redissolution in toluene and precipitation with the addition of methanol.

Transmission electron microscopy (TEM) - TEM images were collected with a TEM Jeol JEM-3010 HR equipped with a LaB6 cathode. Size distribution was calculated using ImageJ 1.53e.[3]

Spectroscopic Characterization

All spectroscopic measurements were performed in anhydrous toluene (spectroscopic grade).

Absorption spectra were recorded in a quartz cell (d = 1 cm) using a JASCO V780 UV-Visible/NIR spectrophotometer (JASCO GmbH, Pfungstadt, Germany). All measurements were performed in a wavelength range of 200 nm to 800 nm. A cuvette with pure solvent was always measured as a reference.

Photoluminescence spectra were recorded in a quartz cell (d = 1 cm) using an FLS980 photoluminescence spectrometer (Edinburgh Instruments Ltd., Livingston, UK) in a 90° geometry. An excitation wavelength of 400 nm was used to record photoluminescence spectra covering a wavelength range of 410 nm to 800 nm. The optical density of the dispersions was set to 0.05-0.10 to avoid inner filter effects and reabsorption of photoluminescence.

The quenching of the PL intensity of the CdSe quantum dots in presence of HM was investigated by adding stepwise small aliquotes (1 µl each) of a HM stock solution in toluene to a QD solution in toluene (3 ml). PL spectra were recorded after each addition. Effects of dilution could be ruled out by a reference measurement by adding similar volumes of pure toluene to a solution of QDs. No decrease in PL intensity was observed under these conditions.

Spectrally resolved photoluminescence decay curves were determined employing a Hamamatsu HPDTA streak camera (C4334, Hamamatsu Photonics K.K., Hamamatsu, Germany). Samples were excited by pulses centered at 390 nm created by frequency-doubling the output of a Ti: sapphire laser (Tsunami, Newport Spectra-Physics GmbH, Berlin, Germany). The repetition rate of the fundamental is reduced to 400 kHz by a pulse selector (model 3980, Newport Spectra-

Physics GmbH, Berlin, Germany). Photoluminescence was collected for solutions from a 1 cm cuvette in a 90° angle and spectrally dispersed on the detector using a CHROMEX spectrograph (Chromex, Albuquerque, NM, USA). The optical density of the solutions was adjusted to circa 0.1 at the excitation wavelength. Measurements were performed with a polarizer set to magic angle, i.e., set to 54.7° with respect to the excitation polarization, in the detection path. A glass plate was used to record the instrumental response function (IRF) by reflecting parts of the attenuated excitation beam directly into the detector. IRFs were typically in the order of 1 ns. The emission was spectrally integrated and the resulting decay traces fitted with DecayFit software.[4] For the investigation of the impact of HM on the PL lifetimes, a series of samples was prepared with similar content of QD but increasing amount to HM.

The fs time-resolved measurements were performed on a system consisting of a Ti: sapphire amplifier (Legend-Elite, Coherent Inc., Santa Clara, CA, USA), producing pulses centered at 795 nm with a repetition rate of 1 kHz and a pulse duration of <100 fs. The pump pulses centered at 390 nm were generated by second harmonic generation from the fundamental. A white light continuum with a spectral range from 340 to 750 nm was generated by focusing a fraction of the fundamental into an eccentrically rotating CaF_2 crystal to probe the sample. The pump pulses were delayed with respect to the probe pulses by means of an optical delay stage (maximum delay: 2 ns) and focused into the sample by a lens (f = 75 cm). The repetition rate of the pump pulses was reduced to 500 Hz by a mechanical chopper and the polarization of the pump with respect to the probe pulses was set to the magic angle (54.7°) using a Berek compensator (Thorlabs GmbH, Bergkirchen, Germany) and a polarizer. The power density of the pump pulse at the sample position was adjusted to 0.2 to 0.6 W cm^{-2}, ensuring 0.6 photon absorptions per QD or less. The white light continuum was split into probe and reference. The probe pulse was focused onto the

sample by a concave mirror (f = 500 mm) and spatially overlapped with the pump pulse. Probe and reference were collected by a detection system (Pascher Instruments AB, Lund, Sweden) consisting of a spectrograph (Acton, Princeton Instruments, Trenton, NJ, USA) equipped with a double-stripe diode array detector. The diode array is read out with the laser repetition rate and the signal (ΔA) is calculated from two consecutive probe pulses, corresponding to pump-on and pump-off conditions. Samples were prepared under inert conditions in a glove box using quartz cuvettes with 1 mm path length, which were additionally closed with parafilm. Samples were stored in a desiccator under inert atmosphere until shortly before the measurement. The sample contained QD and HM in a ratio 1:1. As reference a sample containing the same concentration of QDs in absence of HM was measured. Global fits were performed with a program provided by Jens Uhlig.

Transmission Electron Microscopy

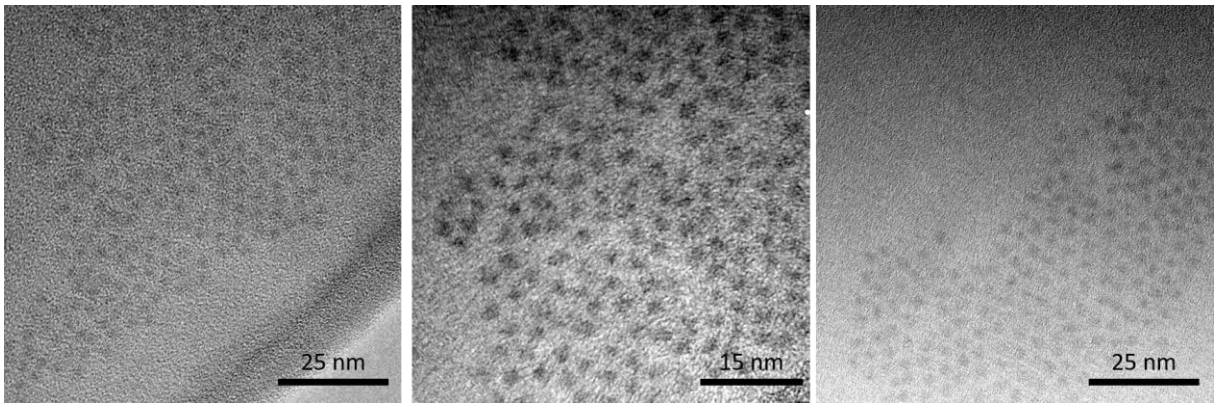

Figure S1. TEM images of the synthesized CdSe quantum dots in different magnifications

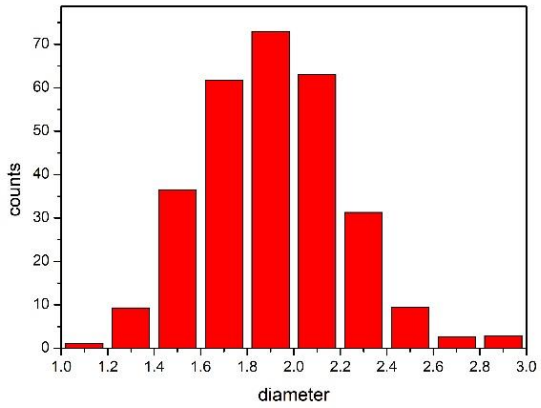

Figure S2. Size distribution determined from the TEM images, mean value 1.9 nm, FWHM 0.7 nm

PL Quenching

For a Stern-Volmer analysis of the PL quenching, both band-edge and trap-state PL was spectrally integrated at different HM concentrations. Then, the ratio of PL in the absence of HM and presence of HM was plotted against HM concentration. The resulting curve (Figure S3) was then fitted with

$$\frac{PL_0}{PL_{HM}} = K_{SV} \times [HM] + y$$

with the integrated PL in the absence of HM PL_0, the integrated PL at the HM concentration [HM] PL_{HM}, the Stern-Volmer constant K_{SV} and the offset y (ideally, y = 1). The curve was only fitted for [HM] < 5 µM and $K_{SV} = (2.0 \pm 0.2) \times 10^6\ M^{-1}$ and y = 0.98 ± 0.04 were obtained.

Deviation from the linear behavior at higher HM concentrations suggests a complex quenching behavior at high concentrations. At low concentrations, most QDs are in contact with only one or less HM molecules. Addition of more HM leads to adsorption of multiple HM molecules to the QD surface and thus complex electron transfer mechanisms in this concentration regime.

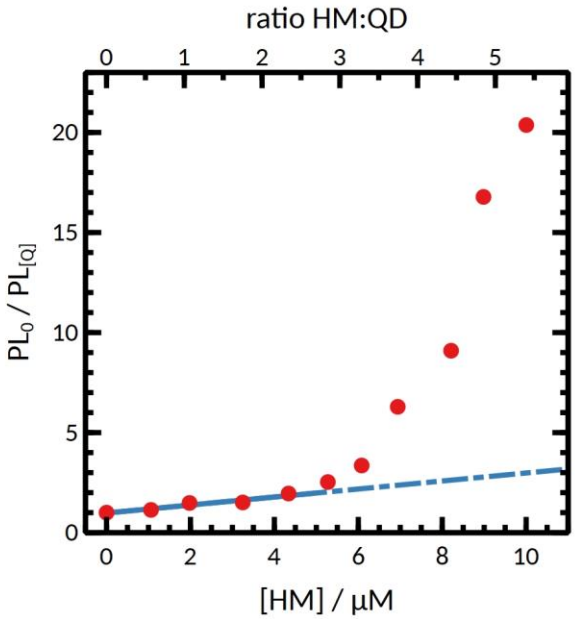

Figure S3. Stern-Volmer plot of the integrated PL intensity over HM concentration. The solid blue line indicates a fit according to the Stern-Volmer equation in the range [HM] = (0,5) µM. The dashed line is a guide to the eye and was not used in the fitting procedure.

PL lifetime measurements

The average lifetime τ_{avg} was calculated via $\tau_{avg} = \tau_1 \times A_1 + \tau_2 \times (1 - A_1)$.

Table **S1.** PL lifetimes and relative amplitudes obtained from a biexponential fit of the PL decays.

Ratio HM:QD ([HM])	**τ_1 / ns (A_1)**	**τ_2 / ns (1-A_1)**	**τ_{avg}/ ns**
0:1 (0 µM)	40 (0.64)	157 (0.35)	82
1:1 (1.98 µM)	33 (0.61)	148 (0.39)	78
2.4:1 (4.34 µM)	41 (0.64)	138 (0.36)	76
3.3:1 (6.08 µM)	41 (0.67)	164 (0.33)	82
4.5:1 (8.21 µM)	44 (0.70)	177 (0.30)	84
5.5:1 (10.00 µM)	35 (0.67)	166 (0.33)	75

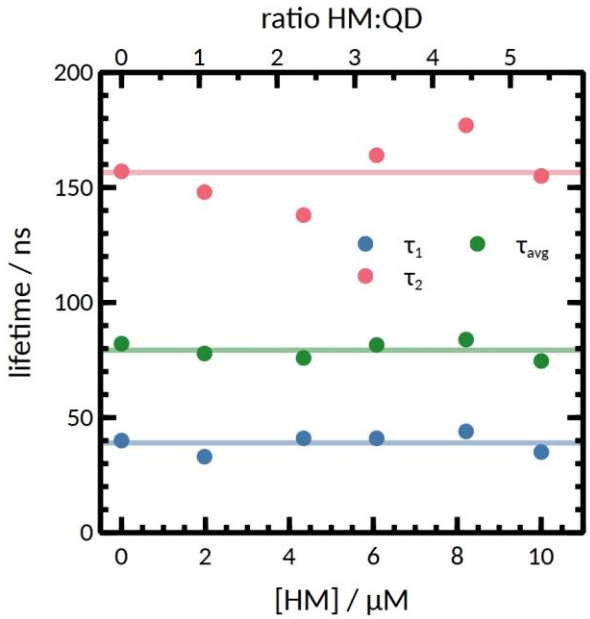

Figure S4. Plot of PL lifetimes obtained from a biexponential fit. Vertical lines represent average lifetimes with ⟨τ_1⟩ = (39 ± 4) ns, ⟨τ_2⟩ = (157 ± 13) ns, and ⟨τ_avg⟩ = (79 ± 4) ns.

Transient Absorption Spectroscopy – Description of fitting procedures

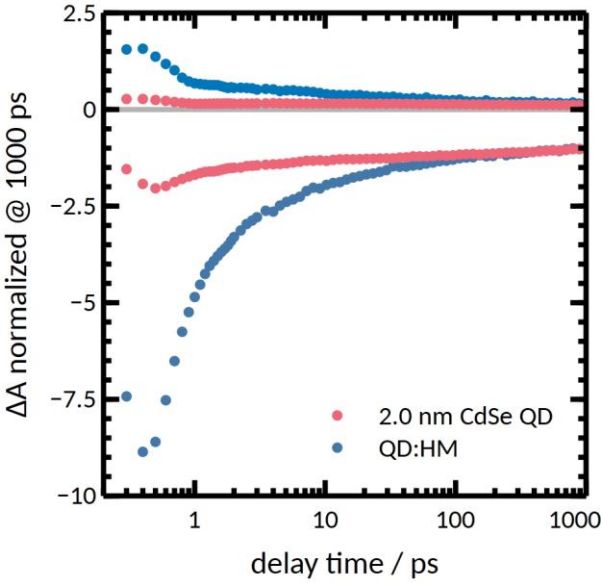

Figure S5. Kinetic traces at 450 and 490 nm recorded for 2.0 nm CdSe QDs in the absence (red) and presence (blue) of HM. These traces have been normalized to the amplitude at a delay time of 1000 ps of pure QDs.

Description of the different fitting models

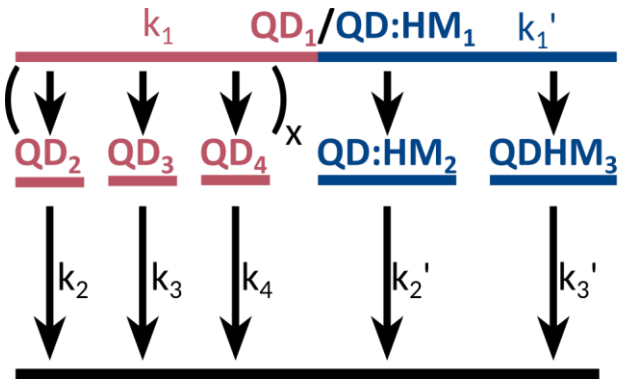

Scheme S1. Kinetic scheme of the fitting model for pure QD and the parallel approach for QD:HM.

For the TA data analysis for pure QDs in toluene, we assumed an initial state QD_1 which is directly populated by the excitation beam g(i), assuming a normally distributed pulse duration in the order of 100 fs. This state decays to *n* other states QD_n, (for the spectral range of 410-500 nm, n = (2,4) and for 550-680 nm n = (2,3)) with a rate constant k_1. Each state QD_n then decays separately from the others with a rate constant k_n. The time-dependent changes in the concentration follows the following rate equations:

$$\frac{d[QD_1]}{dt} = -k_0[QD_1] + g(i)$$

$$\frac{d[QD_n]}{dt} = -k_n[QD_n] + k_1[QD_1]$$

The obtained rates were converted to time constants, which are summarized in Table S2. The kinetic scheme is summarized in Scheme S1. Species-associated spectra are shown in Figure S6.

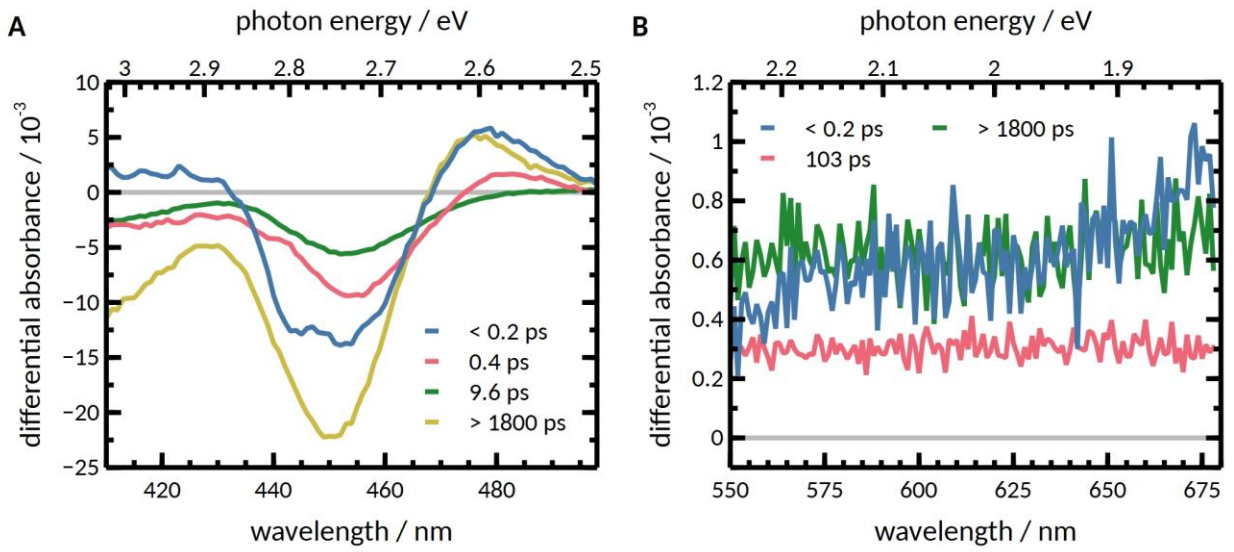

Figure S6. Species-associated spectra of QD in the region of (A) conduction band electron and (B) trapped hole dynamics. Associated time-constants are displayed.

Table S2. Fitting parameters for the kinetic modeling of the electron and hole dynamics in the photoexcited QD.

spectral range	τ_1 / ps	τ_2/ ps	τ_3/ ps	τ_4/ ps
410-500 nm	< 0.2	0.4 ± 0.1	9.6 ± 3.9	4200
550-680 nm	< 0.2	103 ± 8	Offset (>> 1800 ps)	—

For the measurements with the addition of HM, two different approaches were used:

The parallel model has already been applied to nanorods, in which a sub-ensemble was decorated with nanoparticles,[5] and for a molecular Ni catalyst adsorbed to the surface of QDs.[6] An initially excited state *QD:HM*$_1$ is assumed, which is directly populated by the excitation beam g(i), assuming a normally distributed pulse duration in the order of 100 fs. *QD:HM*$_1$ reflects the population of initially excited QDs both in absence and presence of HM. This state then decays to

n other states QD_n, (for the spectral range of 410-500 nm, *n* = (2,4) and for 550-680 nm *n* = (2,3)) scaled by a factor of *x* and *QD:HM*$_m$ (for the spectral range of 410-500 nm, *m* = (2,3) and for 550-680 nm *m* = 2 and with a rate constant k_1'. The states QD_n, then decay with the same rate constants as they were obtained for pure QD, while *QD:HM*$_m$decay with k_m'. The rate equations are as follows

$$\frac{d[QD:HM_1]}{dt} = -k_0'[QD:HM_1] + g(i)$$

$$\frac{d[QD_n]}{dt} = x \cdot (-k_n[QD_n] + k_1'[QD:HM_1])$$

$$\frac{d[QD:HM_m]}{dt} = -k_m'[QD:HM_m] + k_1'[QD:HM_1]$$

For the hole dynamics, k_1' was assumed to be identical to k_1. The obtained rates were converted to time constants, which are summarized in Table S3. The kinetic scheme is summarized in Scheme S1. Species-associated spectra are shown in Figure S7.

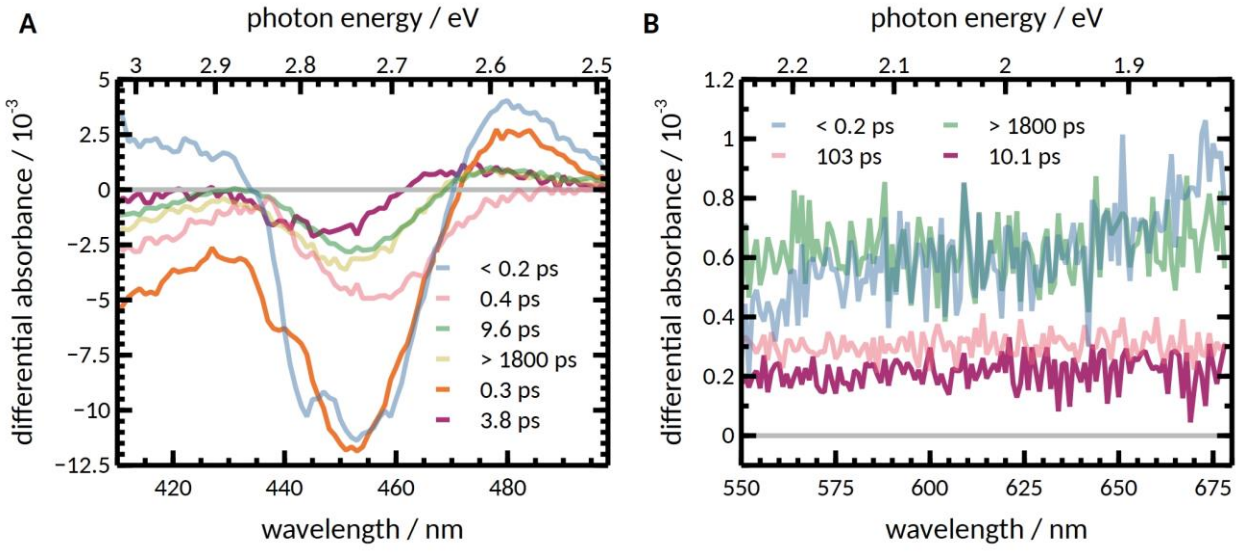

Figure S7. Species-associated spectra of QD:HM obtained using the parallel approach in the region of (A) conduction band electron and (B) trapped hole dynamics. Associated time-constants

are displayed. Spectra obtained for pure QD within this approach are shown as semi-transparent lines.

A conceptually similar approach to the differential model has been used in the modeling of transient absorption data of dye-sensitized nanoparticle films.[7] the difference between transient spectra obtained for the QD:HM complex $TAS(t)_{QD:HM}$ and transient spectra obtained from the fit for pure QD $TAS(t)_{QD,fit}$ was calculated.$TAS(t)_{QD,fit}$ were scaled by

$$x = \frac{\int_{\lambda_1}^{\lambda_2} |TAS(1000ps)_{QD:HM}|}{\int_{\lambda_1}^{\lambda_2} |TAS(1000ps)_{QD,fit}|}$$

which is the ratio of the integral of transient spectra in the wavelength range (λ_1,λ_2) obtained at a delay time of 1000 ps. The obtained data was then fit using the same approach as for pure QD. An additional small offset was included in the fit to accommodate for small deviations stemming from the subtraction of the two datasets. The obtained rates were converted to time constants, which are summarized in Table S3.

Table **S3.** Fitting parameters for the kinetic modeling of the electron and hole dynamics in the photoexcited QD:HM complex using the differential and parallel model.

spectral range	model	τ_1' ps	τ_2'/ ps	τ_3'/ ps	Fraction x
410-500 nm	parallel	< 0.2	0.3 ± 0.1	3.8 ± 1.8	0.22 ± 0.00
	differential	0.3 ± 0.1	2.7 ± 1.6	36.8 ± 8.6	0.18 ± 0.02
550-680 nm	parallel	< 0.2	10.1 ± 0.4	—	0.22 ± 0.13

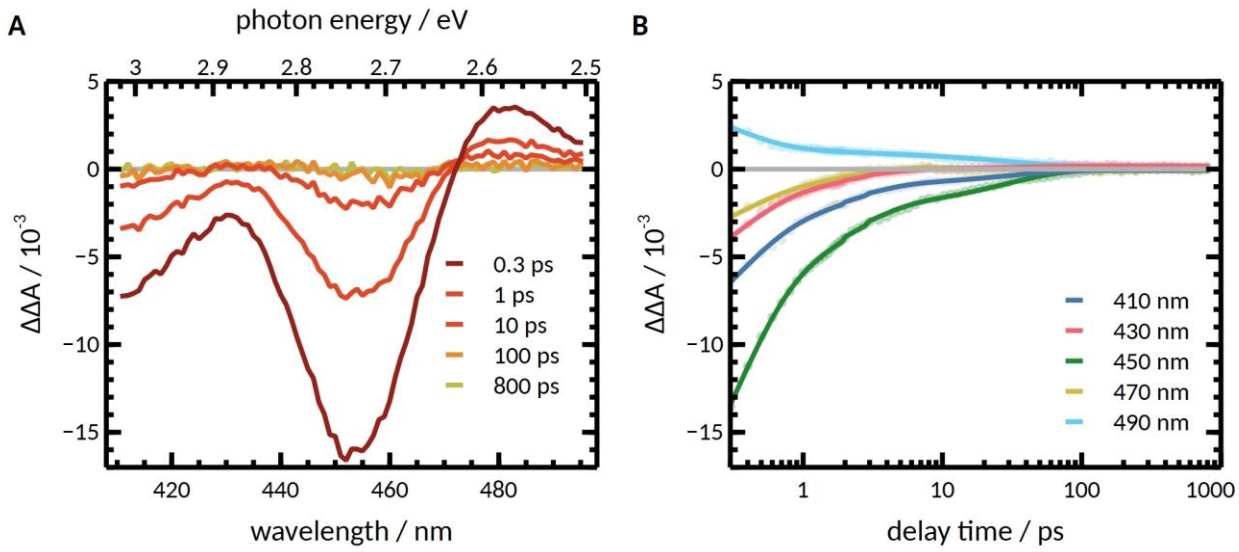

Figure S8. Modeling of the QD:HM excited state dynamics using the "differential" method. A. Transient spectra obtained after scaled subtraction of QD transient spectra from the QD:HM spectra. B. Obtained kinetics using a multiexponential fit (solid lines).

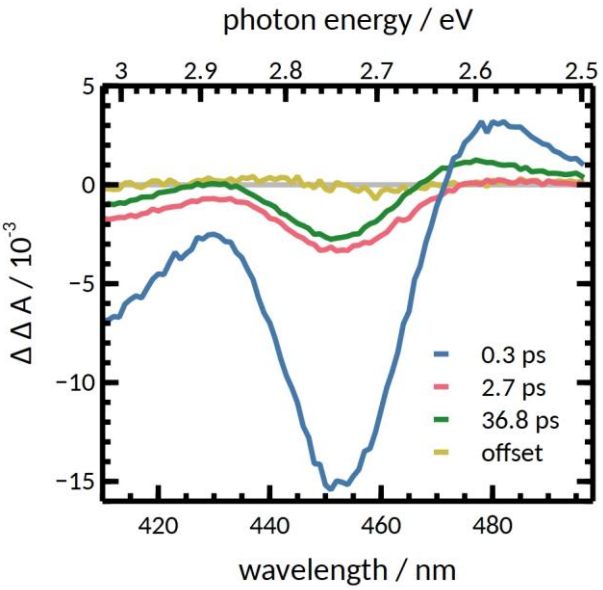

Figure S9. Species-associated spectra of QD:HM obtained using the differential approach in the region of conduction band electron and dynamics. Associated time-constants are displayed.

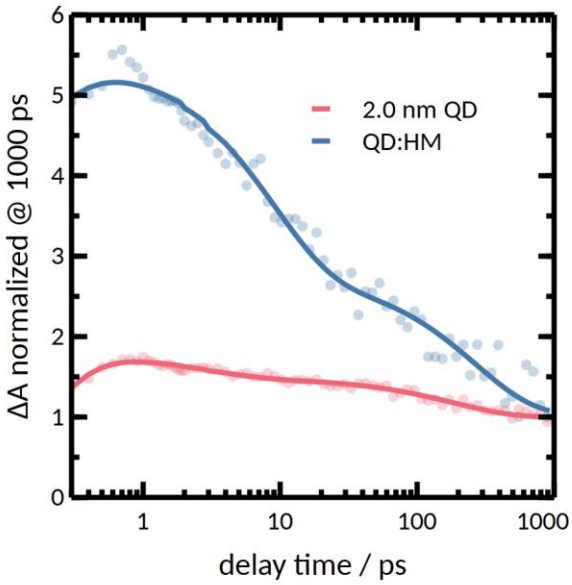

Figure S10. Spectrally integrated kinetic traces between 550 and 680 nm recorded for 2.0 nm CdSe QDs in the absence (red) and presence (blue) of HM. These traces have been normalized to the amplitude at a delay time of 1000 ps of pure QDs.

REFERENCES

(1) Winter, A.; Zsolnai, L.; Huttner, G. Zweikernige und Dreikernige Carbonyleisenkomplexe mit 1.2- und 1.3-Dithiolatobrückenliganden / Dinuclear and Trinuclear Carbonyliron Complexes Containing 1,2-and 1,3-Dithiolato Bridging Ligands. *Zeitschrift für Naturforschung B* **1982**, *37* (11), 1430–1436. https://doi.org/10.1515/znb-1982-1113.

(2) Carbone, L.; Nobile, C.; De Giorgi, M.; Sala, F. D.; Morello, G.; Pompa, P.; Hytch, M.; Snoeck, E.; Fiore, A.; Franchini, I. R.; Nadasan, M.; Silvestre, A. F.; Chiodo, L.; Kudera, S.; Cingolani, R.; Krahne, R.; Manna, L. Synthesis and Micrometer-Scale Assembly of Colloidal CdSe/CdS Nanorods Prepared by a Seeded Growth Approach. *Nano Lett.* **2007**, *7* (10), 2942–2950. https://doi.org/10.1021/nl0717661.

(3) Schneider, C. A.; Rasband, W. S.; Eliceiri, K. W. NIH Image to ImageJ: 25 Years of Image Analysis. *Nature Methods* **2012**, *9* (7), 671–675. https://doi.org/10.1038/nmeth.2089.

(4) FluorTools. *DecayFit - Fluorescence Decay Analysis Software 1.4*; 2014.

(5) Nakibli, Y.; Mazal, Y.; Dubi, Y.; Wächtler, M.; Amirav, L. Size Matters: Cocatalyst Size Effect on Charge Transfer and Photocatalytic Activity. *Nano Lett.* **2018**, *18* (1), 357–364. https://doi.org/10.1021/acs.nanolett.7b04210.

(6) Liu, C.; Qiu, F.; Peterson, J. J.; Krauss, T. D. Aqueous Photogeneration of H2 with CdSe Nanocrystals and Nickel Catalysts: Electron Transfer Dynamics. *J. Phys. Chem. B* **2015**, *119* (24), 7349–7357. https://doi.org/10.1021/jp510935w.

(7) Wahyuono, R. A.; Seidler, B.; Bold, S.; Dellith, A.; Dellith, J.; Ahner, J.; Wintergerst, P.; Lowe, G.; Hager, M. D.; Wächtler, M.; Streb, C.; Schubert, U. S.; Rau, S.; Dietzek, B. Photocathodes beyond NiO: Charge Transfer Dynamics in a π-Conjugated Polymer Functionalized with Ru Photosensitizers. *Scientific Reports* **2021**, *11* (1), 2787. https://doi.org/10.1038/s41598-021-82395-x.